Silicon Photonic Polarization Beam Splitter with Low Loss and High Extinction Ratio Enabled by TOPIC Bends

Alaa Elshazly, Ahmed Bayoumi, Mehmet Oktay, Hakim Kobbi, Rafal Magdziak, Puvendren Subramaniam, Neha Singh, Marko Ersek Filipcic, Maumita Chakrabarti, Dimitrios Velenis, Huseyin Sar, Peter Verheyen, Philippe Absil, Filippo Ferraro, Yoojin Ban, Joris Van Campenhout, Wim Bogaerts, and Qingzhong Deng

***Abstract*—We present a novel compact asymmetric bent directional coupler polarization beam splitter (PBS) fabricated on a silicon-on-insulator (SOI) platform using third-order polynomial interconnected circular (TOPIC) bends. The TOPIC bend design provides continuous curvature and curvature derivatives throughout the structure, which minimizes mode transition losses at connection interfaces. This approach allows for the implementation of tight bend radii to enhance extinction ratio performance without compromising insertion loss, thereby resolving the conventional trade-off limitation in bent-coupler PBS designs. The device performance was characterized through cascaded measurements involving up to 40 PBS units, with single-device loss parameters extracted via linear regression analysis. Comprehensive wafer-level testing across 61 dies confirmed excellent design reproducibility and manufacturing tolerance. The optimized PBS achieves insertion losses as low as 0.017±0.007 dB for TE and 0.019±0.018 dB for TM polarizations, accompanied by extinction ratios of 25.5±0.5 dB and 29.6±6.1 dB, respectively, at 1295 nm wavelength. These results establish new performance benchmarks for silicon photonic PBS devices and demonstrate significant potential for advanced polarization-handling applications in integrated photonic systems.**

***Index Terms*—silicon photonics, polarization management, PBS, low-loss**

I. Introduction

Silicon photonics has emerged as a leading technology for integrated photonic circuits, offering a cost-effective and scalable solution for a wide range of applications. The industry has evolved into a platform that utilizes waveguide technologies to enable the creation of photonic integrated circuits (PICs) [1], [2]. The silicon-on-insulator (SOI) platform, in particular, enables the development of compact and highly integrated devices due to its high refractive index contrast and compatibility with CMOS fabrication processes [3]. This makes SOI-based photonic circuits especially attractive for optical communication systems, where increasing data transmission capacity and integration density are critical. One of the main challenges in SOI-based PICs is the strong birefringence inherent to silicon waveguides, which arises from both geometric and stress-induced factors and leads to significant polarization dependence and can limit device performance [4]. To address this, a range of polarization-handling devices have been developed, including polarization beam splitters (PBSs) which enable the separation and recombination of different polarization states.

Various silicon PBS devices have been implemented utilizing Mach-Zehnder interferometers (MZIs) [5]–[7], Multi-Mode interferometers (MMIs) [8]–[10], Sub-Wavelength Gratings (SWGs) [11], [12], photonic crystals [13], [14], and freeform structures [15]. However, these approaches often come with high insertion loss (IL) of $>$0.5 dB for both polarizations [11]. More recently, there has been growing interest in PBS designs based on Asymmetric Directional Couplers (ADCs) due to its potential for low IL [16]–[32]. The working principle behind ADCs is to introduce geometric asymmetry to a directional coupler so that only one polarization state is phase-matched and thus efficiently coupled, while the other polarization remains phase-mismatched and largely uncoupled. Various ways have been proposed to introduce asymmetry, including slot [16], [17], partially etched [18], [19], and SWG assisted [20]–[22] waveguides. Using these techniques, significant improvements in PBS IL have been achieved, with the lowest reported IL of $0.17(0.22)$ dB for TE(TM) polarization [18]. It is challenging to improve the IL further, as these approaches have added a significant amount

This work was supported by imec's industry-affiliation R&D program "Optical I/O".

A. Elshazly, A. Bayoumi and M. Oktay are with imec, Kapeldreef 75, 3001 Leuven, Belgium and the Photonics Research Group, Department of Information Technology, Ghent University-imec, Ghent, Belgium (email: alaa.elshazly@imec.be; ahmed.bayoumi@ugent.be; mehmet.oktay@imec.be)

H. Kobbi, R. Magdziak, P. Subramaniam, N. Singh, M. E. Filipcic, M. Chakrabarti, D. Velenis, H. Sar, P. Verheyen, P. Absil, F. Ferraro, Y. Ban, J. Van Campenhout, and Q. Deng are with imec, Kapeldreef 75, 3001 Leuven, Belgium (email: hakim.kobbi@imec.be; rafal.magdziak@imec.be; puvendren.subramaniam@imec.be; neha.singh@imec.be; marko.ersekfilipcic@imec.be; maumita.chakrabarti@imec.be; dimitrios.velenis@imec.be; huseyin.sar@imec.be; peter.verheyen@imec.be; philippe.absil@imec.be; filippo.ferraro@imec.be; yoojin.ban@imec.be; joris.vancampenhout@imec.be; qingzhong.deng@imec.be)

W. Bogaerts is with the Photonics Research Group, Department of Information Technology, Ghent University-imec, Ghent, Belgium and IMEC, Kapeldreef 75, 3001 Leuven, Belgium (email: wim.bogaerts@ugent.be)

Corresponding authors: Q. Deng and W. Bogaerts

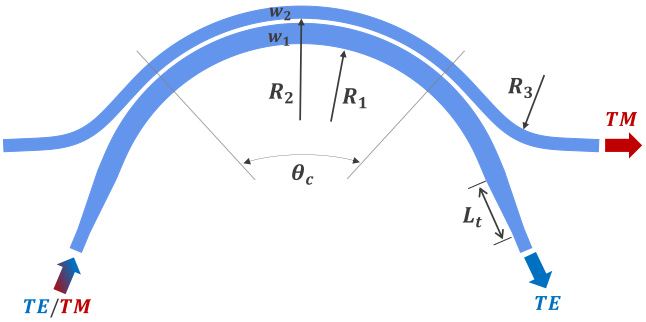

Fig. 1. Schematic of the proposed bent-DC PBS, in which all bends are designed using the TOPIC bend approach.

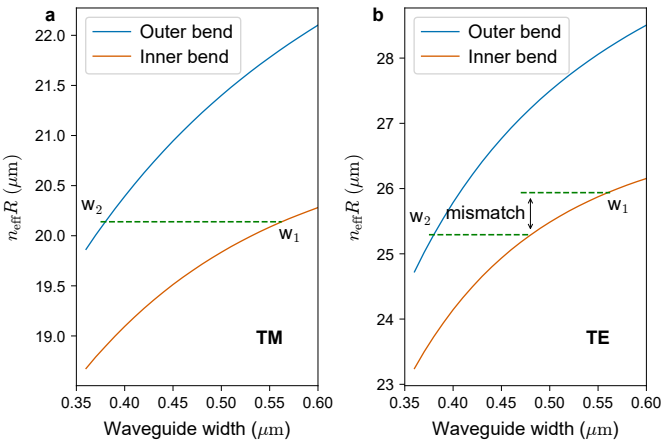

Fig. 2. The $n_{\text{eff}}R$ of the outer and inner bends as a function of waveguide width for (a) TM, and (b) TE mode.

of etched interfaces overlapping with the light, which causes loss through surface roughness from etching.

Another approach to introduce asymmetry is to bend the waveguides [23]–[30]. Bent-DC PBSs have the potential for ultra-low IL because no additional etched interfaces are introduced compared to a straight strip waveguide that is the most commonly used single mode waveguide. However, the practically demonstrated IL is still limited to >0.35(0.1) dB for TE(TM) polarization [30]. The main source of IL is the mode mismatch induced by circular bending. When a waveguide is bent, the light propagating inside it undergoes distortion and shifts toward the outer boundary of the bend, instead of being symmetrically centered as in a straight waveguide [33]. In bent-DC PBSs, these bent waveguides need to be connected with straight waveguides or other bent waveguides with different bending directions as shown in Fig. 1. Mode mismatch losses occur at all these connections. Moreover, the smaller the bend radius, the larger the mode mismatch, and thus the higher the mode mismatch loss. On the other hand, the smaller the bend radius, the larger the phase-mismatch for the uncoupled polarization, and thus the higher the extinction ratio (ER). Different bending strategies have been proposed to mitigate mode transition losses, such as using Euler adiabatic bends [34], [35]; however, no low-loss bends have been introduced to PBSs based on bent-DC. Therefore, there is still an existing trade-off challenge between achieving high ER and low IL in bent-DC PBSs.

In this paper, we propose a bent-DC PBS based on third-order polynomial interconnected circular (TOPIC) bends [33], [36]. The TOPIC bends feature continuous curvature and continuous curvature derivative everywhere, including at all connection points required in a bent-DC PBS, which minimizes mode transition losses. Being freed from mode transition loss constraints, small bend radii can be utilized to achieve high ER while maintaining ultra-low IL. The experimentally demonstrated PBS reported here exhibits an IL of 0.017±0.007 dB with an ER of 25.5±0.5 dB for the TE polarization at peak wavelength, and for TM, an IL of 0.019±0.018 dB and an ER of 29.6±6.1 dB reliably over a wafer-scale measurement.

II. Principle and Theory

As shown in Fig. 1, the proposed bent-DC PBS consists of two parallel bent strip waveguides forming the coupling region, with input and output routing bends for separation. All bends are designed using the TOPIC bend approach with constant width to minimize bend-induced loss [33]. To ensure fabrication compatibility with many popular silicon photonics foundries, the waveguides are designed with 220-nm-thick SOI with silicon oxide as the cladding, and the coupling gap g is set to 250 nm. The outer waveguide width w_2 is fixed to 380 nm, the commonly used single-mode waveguide width in O-band. The outer waveguide radius R_2 is fixed to 10 μm and the routing bend radius R_3 is set to have the radius of 9 μm at the center of the routing waveguides, to enable high-ER potential while no significant bend-induced loss occurs. The inner waveguide width w_1 and the coupling angle θ_c are the free parameters for performance optimization, while the inner waveguide radius R_1 is determined as $R_1 = R_2 - g - w_1$. The inner waveguide width w_1 is optimized to satisfy the phase-matching condition for the TM polarization.

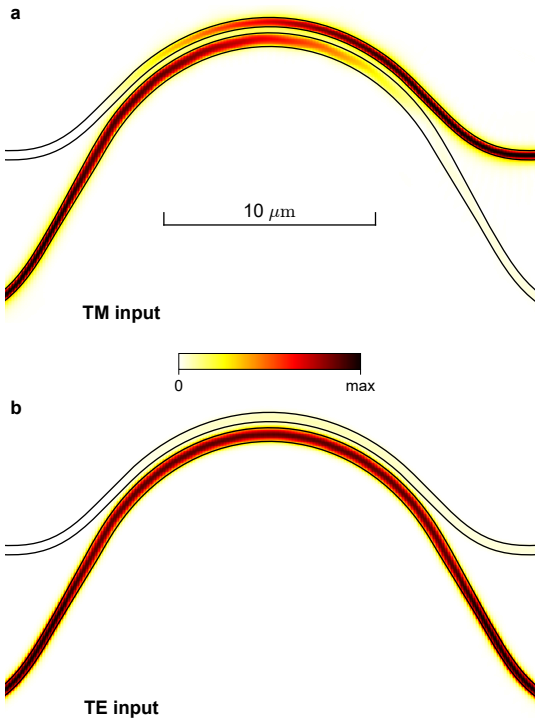

Fig. 3. 3D simulation of the PBS, using COMSOL Multiphysics 6.1, showing the normalized electric field propagation for (a) TM and (b) TE input. The PBS is simulated with an outer bend radius $R_2 = 10$ μm, a routing bend radius R_3 is set to have the radius of 9 μm at the center of the routing waveguides, and coupling gap $g = 0.25$ μm. The outer waveguide width is maintained at $w_2 = 0.38$ μm, while the inner waveguide width is set to the phase-matched width $w_1 = 0.56$ μm. The TOPIC bending angle of the coupling region in the outer waveguide is $\theta_c = 83°$ with a TOPIC transition angle of 5° and circular angle of 73°. The two routing bends in the outer waveguide are also TOPIC bends with a total angle of 45° and transition angle of 22.5°. The inner waveguide taper length is set to $L_t = 3$ μm. To maintain separation between the taper and the coupling region, an additional 30° is added to the circular segment of the inner coupling bend. The material refractive indices of silicon and silicon dioxide are set to 3.5044 and 1.4662, respectively, with a working wavelength of 1310 nm in this simulation. The total PBS footprint is 27×10 μm^2.

This article has been accepted for publication in Journal of Lightwave Technology. This is the author's version which has not been fully edited and content may change prior to final publication. Citation information: DOI 10.1109/JLT.2026.3652920

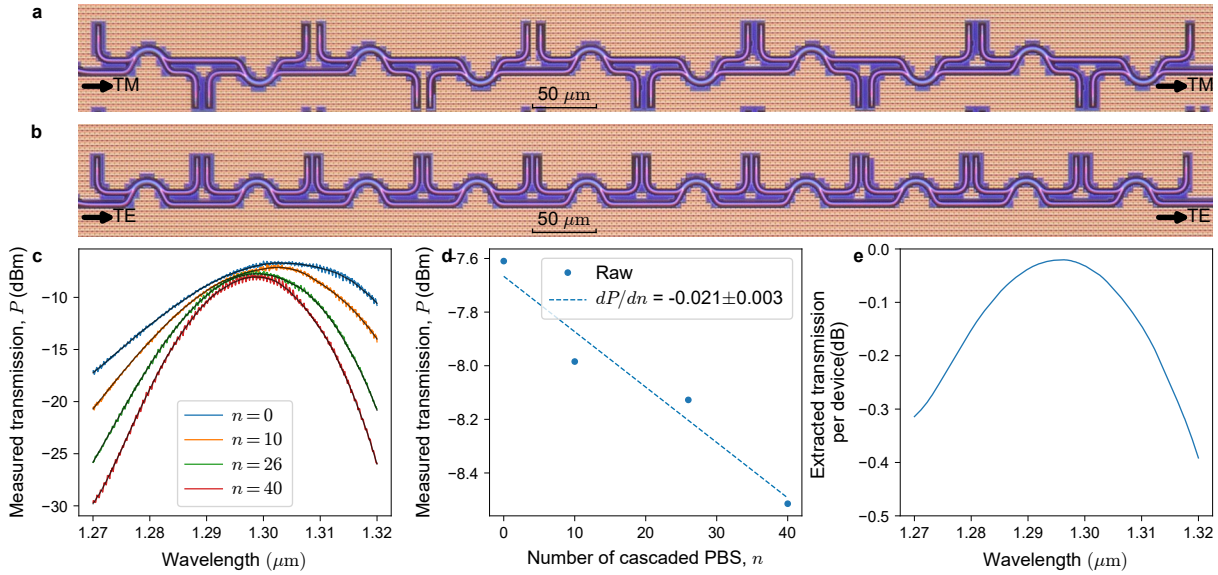

Fig. 4. Microscopic image of the cascading of 10 PBSs for the loss measurement with TM (a) and TE (b) input. (c) The measured raw transmission of the cascaded PBS circuits with denoised trend lines. The colored lines are the raw measurements, while the black lines are denoised by Savitzky-Golay filter. (d) Example of the linear regression performed at wavelength of 1295 nm. (e) Extracted single PBS loss spectrum for TM input.

In order to achieve full coupling for the TM polarization, the phase-matching condition must be satisfied [38], which can be expressed as:

$$n_{\text{eff2}} R_2 = n_{\text{eff1}} R_1, \tag{1}$$

where n_{eff1} and n_{eff2} are the effective indices of the inner and outer coupling bends, respectively. Note that n_{eff} is not well-defined for bent waveguides; therefore, the $n_{\text{eff}} R$ product is used instead. The $n_{\text{eff}} R$ product can be directly calculated from the eigenvalues when the waveguide eigenvalue equation is solved in a cylindrical coordinate system. The simulated values for both TM and TE polarizations as a function of waveguide width are shown in Fig. 2. At $w_2 = 0.38$ μm, the phase-matching condition is satisfied for TM polarization when $w_1 = 0.56$ μm. Simultaneously, a substantial phase-mismatch is maintained for the TE polarization, ensuring minimal cross-coupling for TE input light. To transition this inner waveguide width to the single-mode width of 0.38 μm, a straight taper with a length (L_t) of 3 μm is employed as shown in Fig. 1. The remaining parameter to be optimized is the coupling angle θ_c, which must be set to achieve complete coupling for TM polarized light. As demonstrated by the optical field evolution in Fig. 3, the TM polarization is fully cross-coupled from the bottom input port to the top output port, while the TE polarization pass through the bottom waveguide without significant coupling when the coupling angle is properly selected.

III. Fabrication and Characterization

The proposed PBS was fabricated using imec's most advanced 300 mm silicon photonics platform (iSiPP300), which enables high waveguide quality through 193 nm immersion

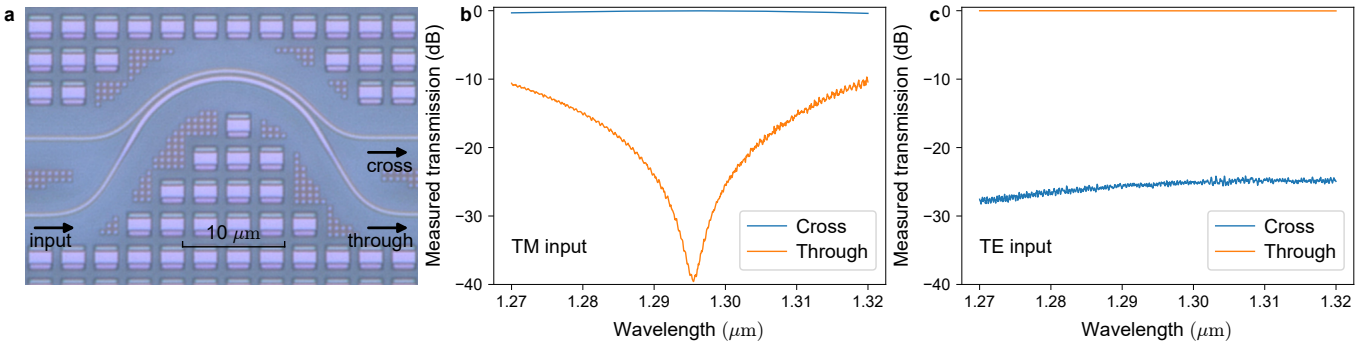

Fig. 5. (a) Microscopic image of the fabricated PBS, with nominal inner waveguide width $w_1 = 0.5$ μm and coupling angle $\theta_c = 95°$ while the other parameters are the same as described in the context earlier. The measured power transmission at the through and cross ports for TM (b), and TE (c) input. In order to be able to handle and measure TM and TE modes, a I/O unit, comprising a TE grating coupler, a TM grating coupler, and the PBS, is employed [37]. The TE grating coupler connects to the top input port of the PBS, while the TM grating coupler connects to the bottom input port. The output is taken from the PBS dominant output, which corresponds to the cross port for TM input and the through port for TE input. An identical unit is mirrored at the output side of the circuit.

This article has been accepted for publication in Journal of Lightwave Technology. This is the author's version which has not been fully edited and content may change prior to final publication. Citation information: DOI 10.1109/JLT.2026.3652920

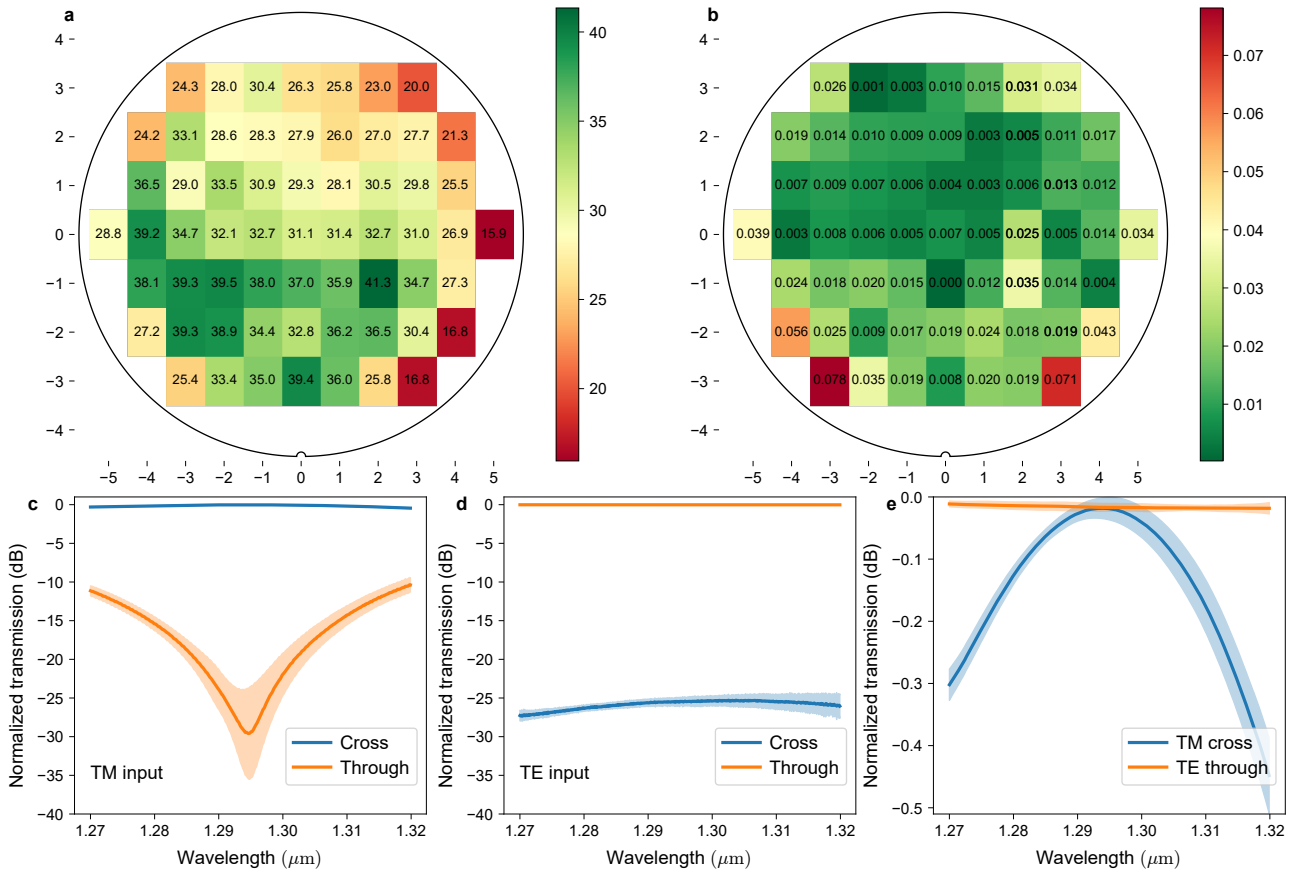

Fig. 6. Wafer maps showing the ER (a), and IL (b) of the TM input at peak wavelength. Wafer-level statistics of the PBS output for TM (c) and TE (d) input, and the zoomed-in view of the dominant outputs (e). The curves are the mean values while the bands with light colors are the standard deviations of the measurements for all 61 dies in one wafer.

lithography. All fabricated waveguides are SOI strip waveguides with a nominal silicon thickness of 220 nm and a 2 μm top oxide cladding layer. To precisely quantify the IL of the PBS, multiple identical PBSs were cascaded to amplify the total loss to a measurable level. Figures 4(a) and 4(b) show microscope images of the cascaded PBS configurations used for IL measurements with TM and TE inputs, respectively. For TM loss measurement, the TM mode couples to the cross port; therefore, the through port is terminated with an inverse taper to prevent back-reflections. The cross port is then routed to the subsequent PBS, which is vertically mirrored to enable compact and efficient routing. For TE loss measurement, transmission is measured directly at the through port, while the cross port is terminated. For TM IL measurement, different numbers (n= 0, 10, 26, and 40) of PBSs were cascaded, with the raw spectra shown in Fig. 4(c). These spectra were then processed using the Savitzky-Golay filter to reduce measurement noise [39]. Subsequently, the transmission of a single PBS at each wavelength was extracted using linear regression analysis on the filtered data, as exemplified in Fig. 4(d) for wavelength 1295 nm. The slope of the linear regression represents the single PBS transmission at that wavelength. The extracted TM transmission spectrum, indicating PBS IL for a single PBS, is shown in Fig. 4(e). For TE IL measurement, the same procedure was followed with n=0 and 40.

PBS ER measurement, on the other hand, is more straightforward. The input light was launched into the bottom input port of the PBS, and the output power was measured at the cross-talk port (through for TM input, and cross for TE input), as shown in Fig. 5(a). The measured PBS transmission spectra are shown in Fig. 5(b) and Fig. 5(c) for TM and TE input light, respectively. The PBS exhibits an ER of 39.5 dB and IL of 0.020 dB at 1295 nm wavelength for TM input. Over the 1270–1320 nm wavelength range, it maintained an ER >10 dB and IL <0.40 dB. The 20-dB bandwidth (BW), defined as the wavelength range with ER>20 dB, of the PBS is around 18 nm. For the TE mode, an IL of 0.008 dB and ER of 25.4 dB were achieved at 1295 nm wavelength; and it maintained excellent performance with an ER >24.5 dB and IL <0.030 dB over the entire measurement range. The spectrum for TM mode shows greater wavelength sensitivity than the TE mode due to the wavelength-dependent nature of evanescent coupling. Since the bent-DC PBS relies on phase-matched coupling for the TM mode, this condition is only met at the center wavelength. As the wavelength deviates from this center point, the phase-matching condition is no longer satisfied, resulting in reduced coupling efficiency, lower ER, and higher IL. This effect is further amplified with larger coupling gaps and longer coupling lengths, resulting from smaller bend radii.

On the other hand, since the TE light propagates directly to the through port without coupling, it exhibits a relatively flat spectral response with excellent performance over the entire measurement range. To the best of our knowledge, this represents the lowest IL reported for a PBS device.

To verify the fabrication tolerance and robustness of the PBS design, measurements were performed on all 61 dies across a single wafer. To visualize performance variations across the wafer, the ER and IL values for the TM mode at peak wavelength are shown in Fig.6(a) and Fig.6(b), respectively. Several outermost edge dies exhibit relatively higher insertion loss and lower ER due to higher process variations that typically occur at the wafer edge. Excluding these outlier edge dies, the TM mode maintains an ER $>$23 dB and IL $<$0.035 dB at peak wavelength across the wafer. The variations in peak ER across the wafer originate from the directional coupler's sensitivity to small geometrical variations, which are amplified by the relatively long coupling length of the PBS, leading to deviations from the phase-matching condition at peak wavelength. From wafer-level measurements, statistical analysis on the transmission spectra for TM and TE input is performed and extracted in Fig.6(c) and Fig.6(d), respectively. The mean and standard deviation are extracted to characterize the statistical performance variations across the wafer. For TM input, the PBS demonstrates an ER of 29.6$\pm$6.1 dB at peak wavelength and maintains a mean ER $>$ 10 dB over the 50 nm measurement wavelength range (1270–1320 nm). For TE input, the PBS maintains excellent performance across all dies with an ER of 25.5$\pm$0.5 dB at peak wavelength and exceeds 24.5 dB over the entire measurement wavelength range.

Fig.6(e) provides a detailed view of the PBS IL variations across dies for both TE and TM modes. For the TM mode at peak wavelength, the IL is 0.019$\pm$0.018 dB, while for the TE mode, it remains at 0.017$\pm$0.007 dB. Over the 1270–1320 nm wavelength range, the mean IL for the TM mode remains below 0.450 dB, while for the TE mode, it remains below 0.020 dB. Overall, these results demonstrate the stability and robustness of the proposed design for large-scale manufacturing. Compared to the literature, our design distinguishes itself as an ultra-low loss PBS, as summarized in Table I. The PBS also demonstrates high ER and excellent fabrication tolerance, making it a practical building block for polarization-diverse photonic circuits and low-loss integrated transceivers. For future improvement, the limited bandwidth of the PBS can be further enhanced by employing a smaller gap and a shorter coupling length, thus reducing the wavelength-dependency resulting in the coupling region. The relation between the coupling length and the bend radius can be further investigated to accommodate the trade-off between the ER and bandwidth. For overall ER improvement, various techniques can be implemented such as adding a sharp bend, which acts as a TM polarizer, or using cascaded bent-DCs [40].

TABLE I
PERFORMANCE COMPARISON OF EXPERIMENTALLY DEMONSTRATED ADC-BASED PBS AT PEAK WAVELENGTH.

Ref.	TE IL (dB)	TM IL (dB)	TE ER (dB)	TM ER (dB)	20dB BW TE/TM (nm)
[25]	0.6	0.3	$>$30	$>$30	90/90
[30]	0.35	0.1	37	46	135/135
[20]	0.31	0.3	19	40	-/60
[18]	0.17	0.22	30	40	175/175
[26]	$>$0.1	$>$0.1	$>$20	$>$20	90/-
This work	0.017$\pm$0.007	0.019$\pm$0.018	25.5$\pm$0.5	29.6$\pm$6.1	50/18

IV. CONCLUSION

We have demonstrated a bent-DC PBS with ultra-low insertion loss while maintaining high extinction ratio. A novel low-loss TOPIC bend was employed to minimize bending and transition losses, enabling the use of small bend radii without compromising performance. To accurately evaluate the ultra-low insertion loss, up to 40 PBS devices were cascaded, and the loss of a single PBS was extracted using linear regression analysis. The fabricated PBS performance was characterized across the entire wafer to provide an accurate assessment of the design robustness and fabrication tolerance. The PBS demonstrated excellent performance, achieving an IL of 0.017$\pm$0.007 dB and ER of 25.5$\pm$0.5 dB for TE input, and an IL of 0.019$\pm$0.018 dB with ER of 29.6$\pm$6.1 dB for TM input at peak wavelength. To the best of our knowledge, this represents the lowest insertion loss ever reported for a PBS device in silicon photonics. The proposed PBS design is therefore well-suited as an efficient low-loss building block for polarization-diverse circuits in high-density optical communication systems.

REFERENCES

[1] C. Li, M. Zhang, H. Xu, Y. Tan, Y. Shi, and D. Dai, "Subwavelength silicon photonics for on-chip mode-manipulation," *PhotoniX*, vol. 2, no. 1, p. 11, Jul. 2021. [Online]. Available: https://doi.org/10.1186/s43074-021-00032-2

[2] D. Shahwar, H. H. Yoon, S.-T. Akkanen, D. Li, S. t. Muntaha, M. Cherchi, T. Aalto, and Z. Sun, "Polarization management in silicon photonics," *npj Nanophotonics*, vol. 1, no. 1, Sep. 2024.

[3] Y. Su, Y. Zhang, C. Qiu, X. Guo, and L. Sun, "Silicon Photonic Platform for Passive Waveguide Devices: Materials, Fabrication, and Applications," *Advanced Materials Technologies*, vol. 5, no. 8, p. 1901153, 2020, zSCC: 0000015 _eprint: https://onlinelibrary.wiley.com/doi/pdf/10.1002/admt.201901153 tex.ids= su_silicon_2020-1.

[4] D. Dai, L. Liu, S. Gao, D.-X. Xu, and S. He, "Polarization management for silicon photonic integrated circuits," *Laser & Photonics Reviews*, vol. 7, no. 3, pp. 303–328, 2013, zSCC: 0000272 _eprint: https://onlinelibrary.wiley.com/doi/pdf/10.1002/lpor.201200023.

[5] D. Dai, Z. Wang, J. Peters, and J. E. Bowers, "Compact Polarization Beam Splitter Using an Asymmetrical Mach–Zehnder Interferometer Based on Silicon-on-Insulator Waveguides," *IEEE Photonics Technology Letters*, vol. 24, no. 8, pp. 673–675, Apr. 2012. [Online]. Available: https://ieeexplore.ieee.org/document/6132406

[6] S. Gao, Y. Wang, K. Wang, and E. Skafidas, "Low-Loss and Broadband 2 \times 2 Polarization Beam Splitter Based on Silicon Nitride Platform," *IEEE Photonics Technology Letters*, vol. 28, no. 18, pp. 1936–1939, Sep. 2016. [Online]. Available: https://ieeexplore.ieee.org/document/7486036

[7] S. Guerber, C. Alonso-Ramos, D. Benedikovic, E. Durán-Valdeiglesias, X. Le Roux, N. Vulliet, E. Cassan, D. Marris-Morini, C. Baudot, F. Boeuf, and L. Vivien, "Broadband Polarization Beam Splitter on a Silicon Nitride Platform for O-Band Operation," *IEEE Photonics Technology Letters*, vol. 30, no. 19, pp. 1679–1682, Oct. 2018. [Online]. Available: https://ieeexplore.ieee.org/document/8450620

[8] A. Hosseini, S. Rahimi, X. Xu, D. Kwong, J. Covey, and R. Chen, "Ultracompact and fabrication-tolerant integrated polarization splitter," *Optics letters*, vol. 36, pp. 4047–9, Oct. 2011.

[9] M. Yin, W. Yang, Y. Li, X. Wang, and H. Li, "CMOS-compatible and fabrication-tolerant MMI-based polarization beam splitter," *Optics Communications*, vol. 335, pp. 48–52, Jan. 2015. [Online]. Available: https://www.sciencedirect.com/science/article/pii/S0030401814008219

[10] Y. D'Mello, E. El-Fiky, J. Skoric, A. Kumar, M. Hui, Y. Wang, L. Guenin, D. Patel, and D. V. Plant, "Compact, Angled Polarization Splitter: Characterization of Broadband Performance and Fabrication Tolerance," *IEEE Photonics Journal*, pp. 1–1, 2018. [Online]. Available: https://ieeexplore.ieee.org/document/8516338/

[11] H. Xu, D. Dai, and Y. Shi, "Ultra-Broadband and Ultra-Compact On-Chip Silicon Polarization Beam Splitter by Using Hetero-Anisotropic Metamaterials," *Laser & Photonics Reviews*, vol. 13, Feb. 2019.

[12] J. Luque-González, a. herrero, A. Ortega-Moñux, M. Sánchez-Rodríguez, A. Velasco, J. Schmid, P. Cheben, I. Molina-Fernández, and R. Halir, "Polarization splitting directional coupler using tilted subwavelength gratings," *Optics Letters*, vol. 45, May 2020.

[13] U. G. Yasa, M. Turduev, I. H. Giden, and H. Kurt, "High Extinction Ratio Polarization Beam Splitter Design by Low-Symmetric Photonic Crystals," *Journal of Lightwave Technology*, vol. 35, no. 9, pp. 1677–1683, May 2017. [Online]. Available: https://ieeexplore.ieee.org/document/7833079

[14] L. Xu, Y. Wang, E. El-Fiky, D. Mao, A. Kumar, Z. Xing, M. G. Saber, M. Jacques, and D. V. Plant, "Compact Broadband Polarization Beam Splitter Based on Multimode Interference Coupler With Internal Photonic Crystal for the SOI Platform," *Journal of Lightwave Technology*, vol. 37, no. 4, pp. 1231–1240, Feb. 2019. [Online]. Available: https://ieeexplore.ieee.org/document/8598856/citations#citations

[15] L. H. Frandsen and O. Sigmund, "Inverse design engineering of all-silicon polarization beam splitters," in *Photonic and Phononic Properties of Engineered Nanostructures VI*, vol. 9756. SPIE, Mar. 2016, pp. 48–53. [Online]. Available: https://www.spiedigitallibrary.org/conference-proceedings-of-spie/9756/97560Y/Inverse-design-engineering-of-all-silicon-polarization-beam-splitters/10.1117/12.2210848.full

[16] S. Lin, J. Hu, and K. B. Crozier, "Ultracompact, broadband slot waveguide polarization splitter," *Applied Physics Letters*, vol. 98, no. 15, Apr. 2011.

[17] S. Mao, L. Cheng, C. Zhao, and H. Y. Fu, "Ultra-broadband and ultra-compact polarization beam splitter based on a tapered subwavelength-grating waveguide and slot waveguide," *Optics Express*, vol. 29, no. 18, p. 28066, Aug. 2021.

[18] Y. Tian, J. Qiu, C. Liu, S. Tian, Z. Huang, and J. Wu, "Compact polarization beam splitter with a high extinction ratio over S + C + L band," *Optics Express*, vol. 27, no. 2, pp. 999–1009, Jan. 2019. [Online]. Available: https://opg.optica.org/oe/abstract.cfm?uri=oe-27-2-999

[19] Y. Huang, X. Zou, C. Xie, and Y. Zhang, "Ultrahigh extinction ratio and ultralow insertion loss for polarization beam splitter based on two folded asymmetrical directional couplers with dual-stage etching," *Applied Optics*, vol. 62, no. 4, p. 965, Jan. 2023.

[20] Ang, Hang, Iajiu, heng, Ipeng, ong, Eixi, iu, Eipeng, rka, and Ajumdar, "Ultra-broadband and compact polarizing beam splitter in silicon photonics," 2020. [Online]. Available: https://www.semanticscholar.org/paper/Ultra-broadband-and-compact-polarizing-beam-in-Ang-Hang/4501d32021cb764a1d466f41d2a77799943d7f9b

[21] C. Li, M. Zhang, J. E. Bowers, and D. Dai, "Ultra-broadband polarization beam splitter with silicon subwavelength-grating waveguides," *Optics Letters*, vol. 45, no. 8, pp. 2259–2262, Apr. 2020.

[22] S. Z. Ahmed, I. Ahmed, M. B. Mia, N. Jaidye, and S. Kim, "Ultra-high extinction ratio polarization beam splitter with extreme skin-depth waveguide," *Optics Letters*, vol. 46, no. 9, p. 2164, Apr. 2021.

[23] J. Wang, D. Liang, Y. Tang, D. Dai, and J. E. Bowers, "Realization of an ultra-short silicon polarization beam splitter with an asymmetrical bent directional coupler." *Optics letters*, vol. 38, no. 1, pp. 4–6, 2013.

[24] N. Zhao, C. Qiu, Y. He, Y. Zhang, and Y. Su, "Broadband polarization beam splitter by using cascaded tapered bent directional couplers," *IEEE Photonics Journal*, vol. 11, no. 4, pp. 1–8, Aug. 2019.

[25] J. R. Ong, T. Y. L. Ang, E. Sahin, B. Pawlina, G. F. R. Chen, D. T. H. Tan, S. T. Lim, and C. E. Png, "Broadband silicon polarization beam splitter with a high extinction ratio using a triple-bent-waveguide directional coupler," *Optics Letters*, vol. 42, no. 21, p. 4450, oct 2017.

[26] T. Y. L. Ang, J. R. Ong, S. T. Lim, B. Pawlina, E. Sahin, C. E. Png, H. S. Chu, G. F. R. Chen, and D. T. H. Tan, "Broadband silicon bridge waveguide polarization beam splitter," in *Silicon Photonics XII*, G. T. Reed and A. P. Knights, Eds., vol. 10108. SPIE, Feb. 2017, p. 101080A.

[27] N. Zhao, Y. He, C. Qiu, Y. Zhang, and Y. Su, "Ultra-broadband Polarization Beam Splitter Based on a Tapered Bent Directional Coupler," in *2018 Asia Communications and Photonics Conference (ACP)*, Oct. 2018, pp. 1–3. [Online]. Available: https://ieeexplore.ieee.org/document/8596254

[28] H. Wu and D. Dai, "High-Performance Polarizing Beam Splitters Based on Cascaded Bent Directional Couplers," *IEEE Photonics Technology Letters*, vol. 29, no. 5, pp. 474–477, Mar. 2017. [Online]. Available: https://ieeexplore.ieee.org/document/7831419

[29] J. Zhu, H. Huang, Y. Zhao, Y. Li, X. She, H. Liao, R. Huang, Z. Zhu, X. Liu, Z. Sheng, and F. Gan, "Ultra-Compact Mode (De)Multiplexer and Polarization Beam Splitter Based on Tapered Bent Asymmetric Directional Couplers," *IEEE Photonics Journal*, vol. 14, no. 1, pp. 1–6, Feb. 2022. [Online]. Available: https://ieeexplore.ieee.org/document/9653835

[30] H. Wu, Y. Tan, and D. Dai, "Ultra-broadband high-performance polarizing beam splitter on silicon," *Optics Express*, vol. 25, no. 6, p. 6069, Mar. 2017.

[31] P.-H. Fu, T.-Y. Huang, K.-W. Fan, and D.-W. Huang, "Optimization for Ultrabroadband Polarization Beam Splitters Using a Genetic Algorithm," *IEEE Photonics Journal*, vol. 11, no. 1, pp. 1–11, Feb. 2019. [Online]. Available: https://ieeexplore.ieee.org/document/8579194

[32] W. Chen, B. Zhang, P. Wang, S. Dai, W. Liang, H. Li, Q. Fu, J. Li, Y. Li, T. Dai, H. Yu, and J. Yang, "Ultra-compact and low-loss silicon polarization beam splitter using a particle-swarm-optimized counter-tapered coupler," *Optics Express*, vol. 28, no. 21, pp. 30 701–30 709, Oct. 2020. [Online]. Available: https://opg.optica.org/oe/abstract.cfm?uri=oe-28-21-30701

[33] Q. Deng, A. H. El-Saeed, A. Elshazly, G. Lepage, C. Marchese, P. Neutens, H. Kobbi, R. Magdziak, J. De Coster, J. R. Vaskasi, M. Kim, Y. Tong, N. Singh, M. E. Filipcic, P. Van Dorpe, K. Croes, M. Chakrabarti, D. Velenis, P. De Heyn, P. Verheyen, P. Absil, F. Ferraro, Y. Ban, and J. Van Campenhout, "Low-loss and low-power silicon ring based wdm 32×100 ghz filter enabled by a novel bend design," *Laser & Photonics Reviews*, vol. 19, no. 5, Nov. 2024.

[34] H. Zafar and M. F. Pereira, "An efficient and compact mid-infrared polarization splitter and rotator based on a bifurcated tapered-bent waveguide," *Scientific Reports*, vol. 15, no. 1, Feb. 2025.

[35] ——, "A novel mid-infrared transverse magnetic mode pass periodic waveguide polarizer with low reflections," *IEEE Access*, vol. 12, pp. 48 294–48 300, 2024.

[36] A. H. El-Saeed, A. Elshazly, H. Kobbi, R. Magdziak, G. Lepage, C. Marchese, J. R. Vaskasi, S. Bipul, D. Bode, M. E. Filipcic, D. Velenis, M. Chakrabarti, P. De Heyn, P. Verheyen, P. Absil, F. Ferraro, Y. Ban, J. Van Campenhout, W. Bogaerts, and Q. Deng, "Low-loss silicon directional coupler with arbitrary coupling ratios for broadband wavelength operation based on bent waveguides," *Journal of Lightwave Technology*, vol. 42, no. 17, pp. 6011–6018, Sep. 2024.

[37] Q. Deng, M. Jin, J. Qin, P. Sun, H. Shu, C. Ju, P. Neutens, Z. Tao, P. Zhou, B. Wang, Y. Tao, X. Zhang, J. Shi, B. Bai, L. Liu, X. Xiao, P. Van Dorpe, X. Wang, and Z. Zhou, "On-chip light polarization management by mapping the polarization information to phase shift," *Laser & Photonics Reviews*, vol. 18, no. 1, p. 2300501, Nov. 2024.

[38] D. Dai and J. E. Bowers, "Novel ultra-short and ultra-broadband polarization beam splitter based on a bent directional coupler," *Optics Express*, vol. 19, no. 19, pp. 18 614–18 620, Sep. 2011. [Online]. Available: https://opg.optica.org/oe/abstract.cfm?uri=oe-19-19-18614

[39] A. Savitzky and M. J. E. Golay, "Smoothing and differentiation of data by simplified least squares procedures." *Analytical Chemistry*, vol. 36, no. 8, pp. 1627–1639, 1964. [Online]. Available: https://doi.org/10.1021/ac60214a047

[40] H. Zafar and M. F. Pereira, "Recent progress in light polarization control schemes for silicon integrated photonics," *Laser and Photonics Reviews*, vol. 18, no. 11, Jun. 2024.